Optical system for closed-loop testing of adaptive optic convex mirror

Roland J. Sarlot[a], James H. Burge[ab]

[a]Steward Observatory, University of Arizona, Tucson, AZ 85721
[b]Optical Sciences Center, University of Arizona, Tucson, AZ 85721

ABSTRACT

Steward Observatory is building a deformable f/15 secondary mirror for the 6.5 m Multiple Mirror Telescope conversion that will compensate for atmospheric turbulence. A potential difficulty of an adaptive secondary mirror is the ability to verify the commanded mirror shapes of a large convex deformable surface. A new optical design is presented to test the deformable mirror's closed loop control system by optically projecting an artificial star to simulate starlight in the actual telescope. An optical fiber fed interferometer has been incorporated into the design to measure the deformable mirror's ability to compensate for atmospheric turbulence by measuring the wavefront through an atmospheric turbulence generator. The test system has been designed to verify the control system by fitting into both a laboratory test structure as well as the telescope support structure itself. The optical design relies on two wavelength computer generated holograms used to remove spherical aberration as well as aid in the alignment of the test system optics by projecting alignment patterns.

Keywords: adaptive optics, aspheric testing, Multiple Mirror Telescope, interferometry

1. BACKGROUND

The University of Arizona's 6.5m Multiple Mirror Telescope (MMT) conversion will correct atmospheric turbulence by actively deforming the 64 cm f/15 secondary mirror with 336 actuators directly mounted to the back of the mirror. This adaptive secondary mirror provides a fully corrected image to the scientific instrument without the need for extra relay surfaces and their associated efficiency losses and increases in thermal background. The telescope images will be corrected with an adaptive optic system which utilizes a laser beacon produced by exciting sodium atoms in the upper atmosphere and a dimmer natural guide star which compensates for global tip/tilt. The visible laser beacon is then imaged onto a wavefront sensor for shape control and the infrared guide star will control tip/tilt through the use of quad cells. The Shimmulator, a complete optical system, is being built to allow closed-loop testing of the active compensation system and includes methods to verify the commanded secondary mirror shapes. Testing the closed-loop system in the laboratory will reserve expensive telescope time for observing rather than calibrating and testing. The design of this system required an innovative solution to provide multi-wavelength simulation of starlight reflecting off the secondary mirror analogous to the reflection in the telescope. A conceptual illustration comparing the MMT and the Shimmulator design is depicted in figure 1.

2. DESIGN OBJECTIVES

The Shimmulator had to be designed to comply with multiple constraints. It had to use a single reflection off the convex aspheric secondary mirror and bring the light to focus on the wavefront sensor, simulating starlight in the actual telescope. In particular, the optical design specifications had an implied unique requirement -- that the secondary aspheric mirror, with intrinsic power, be tested within the optical system and image the fiber source to the image plane. The test system also had physical constraints in order to operate in the lab as well as fit within the MMT structure and not intrude into the wavefront sensing optics nor the visible cameras. The physical constraints also required the image plane of the MMT f/15 and the test optics to be coincident. The mapping of the secondary onto the wavefront sensor must be controlled to less than 10% of the actuator spacing to accurately correct the atmospheric turbulence. This equates to a mapping accuracy of 2 mm on the secondary mirror. Another mapping requirement was the CGH to the secondary which was required to be less than 2% mismatch. To minimize downtime assembling the adaptive system, two adaptive secondary mirrors are being built – a spherical prototype and the MMT hyperboloidal mirror, and it was desired that the same Shimmulator setup test both mirrors with minimal changes. The two-tiered control system uses infrared light on a quad cell in the main science instrument for tip/tilt compensation and the visible (589 nm) laser beacon on a 13 x 13 element Shack-Hartmann array for wavefront correction, therefore, the Shimmulator must provide simultaneous dual wavelength operation. Additionally, the dual

Part of the SPIE Conference on Novel Optical Systems Design and Optimization II • San Diego, California • July 1998
SPIE Vol. 3430 • 0277-786X/98/$10.00

wavelength operation will allow testing of the infrared science cameras during closed loop operations of the adaptive optic system. The optical test demanded a field size greater than 5.6 arcseconds in the same position as the telescope focus. The Shimmulator must simulate turbulence following Kolmogorov statistics to measure the system's ability to correct atmospheric-like disturbances and residual errors. Finally, the design had to incorporate an interferometer to allow accurate measurement of the commanded mirror shape errors.

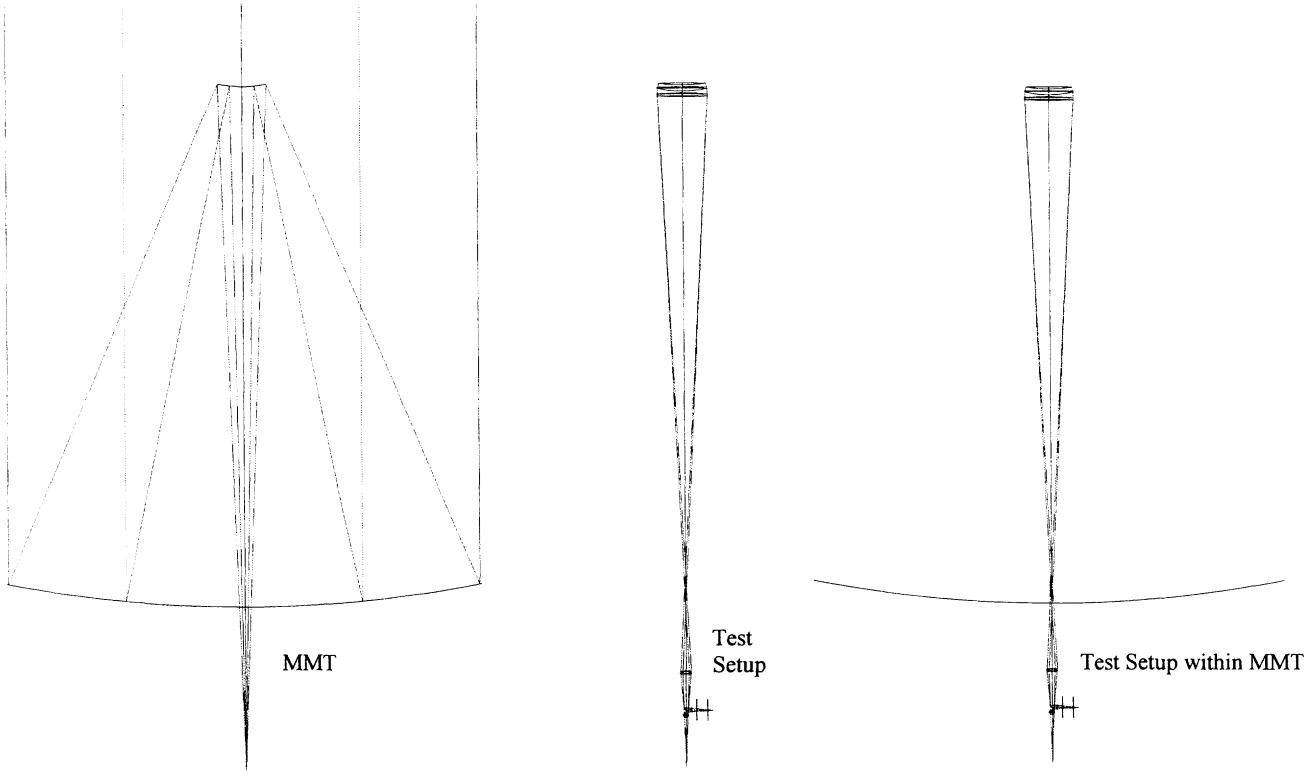

Figure 1. The MMT and the test optics have completely different source paths. The MMT images starlight from infinity and the test setup projects light from an optical fiber, yet the reflected light from the secondary mirror arriving at the image plane for both setups is equivalent. Note that the Shimmulator optics can be inserted into the MMT optical path to test the secondary mirror in situ.

3. Optical Design

The full path optical design solution that is currently being fabricated is shown in Figure 2. A fiber fed light source is projected through the atmospheric turbulence generator. The light source then passes through a fused silica substrate with a computer generated hologram written on the back surface before reflecting off the beam splitter and passes through the doublet. Nearly 8 m away, before the light reflects off the secondary, there are two 700 mm diameter BK7 lenses. These lenses essentially neutralize the convexity of the secondary and guide the light back towards the image plane. The doublet acts as a mapping compensator for both wavelengths. Detail of the large lenses is illustrated in Figure 3; the optical components near the source are detailed in Figure 4.

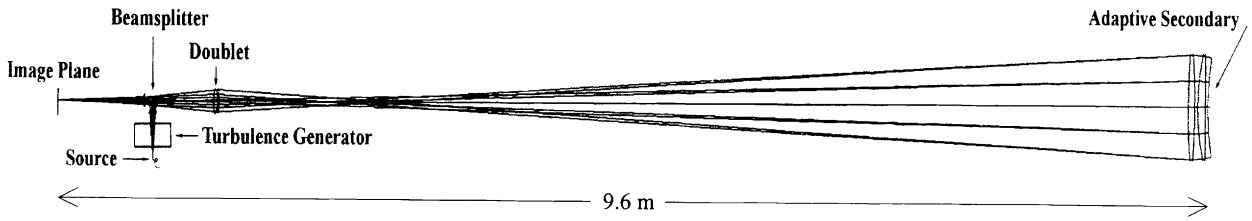

Figure 2. The Shimmulator optical design is drawn with the image plane to the left, the fiber fed light source directed upwards through the atmospheric turbulence generator at the bottom left and the adaptive secondary to the extreme right.

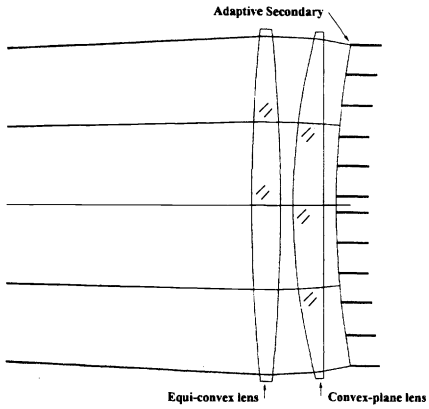

Figure 3. The adaptive aspheric secondary is represented on the right with actuators supporting the surface shape. The two large lenses are approximately 700 mm in diameter with 20 mm edge thicknesses.

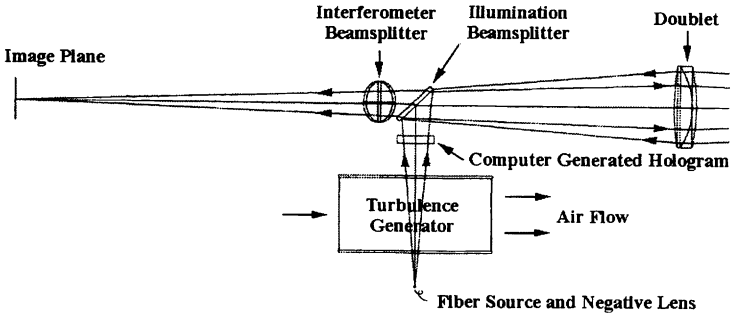

Figure 4. The illustration highlights the optical components of the Shimmulator near the source and image end. The bottom of the figure contains the fiber source which is immediately followed with a negative lens before the light enters the turbulence generator and proceeds to the computer generated hologram.

The optical paths for both wavelengths are completely different. Although the optical elements and spacings are identical, Figures 5 illustrates the beam paths for both wavelengths with the only difference being a 24 mm decrease in the back focal distance for the visible design. Additionally, testing either the aspherical or the spherical secondary mirror does not require any changes in the optical setup other than a single change of holograms.

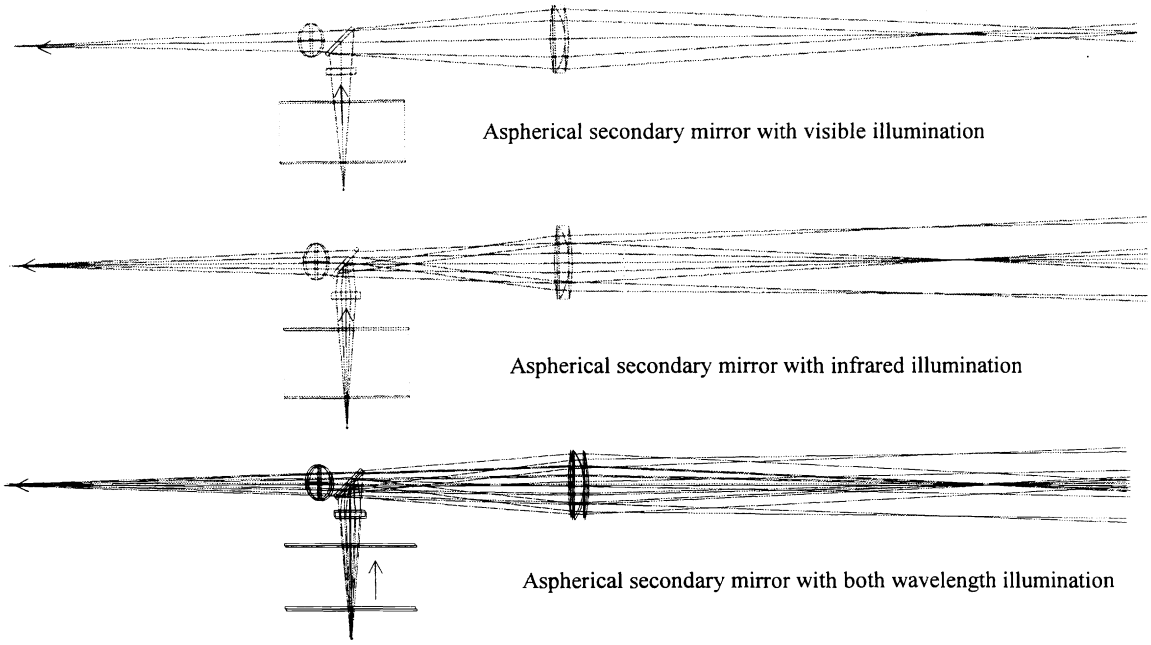

Figure 5. The above two illustrations trace the ray paths through each of the two illumination wavelengths for the aspherical secondary test. The ray paths through the configurations are significantly different yet the rays converge with equivalent residual mapping error and at the same image location as the MMT f/15 focus. The lower illustration traces both wavelengths simultaneously through the system as they will follow in the actual system.

The design mapping requirements were such that upon looking at the adaptive secondary mirror from the f/15 focus position of the MMT, no secondary actuator would appear displaced more than 2 mm when the Shimmulator optics were inserted between the secondary mirror and the f/15 focus. The mapping error constraint was balanced with the wavelength mismatch on the secondary. The wavelength mismatch measures points on the secondary between the two wavelengths in pupil space since the hologram location and the secondary mirror are conjugates. The design residual mapping error at the wavefront sensor was less than the 2 mm displacement for any point over the mirror surface and is graphed in Figure 6.

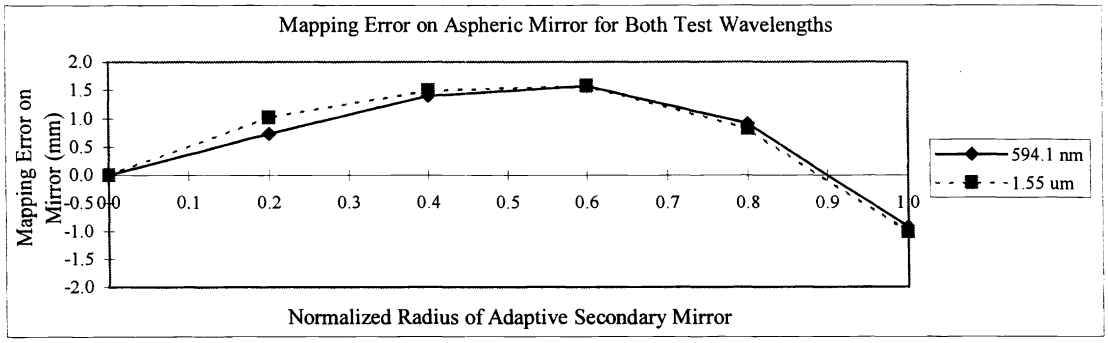

Figure 6. Graph of the mapping error for both wavelengths in the Shimmulator design. The horizontal axis is normalized across the adaptive secondary and the height scale represents the mapping error from the nominal position.

Table 1 lists the nominal system performance as compared to the system specifications.

Design Requirement	Specification	Nominal Design
Simultaneous two wavelength operation	593.96 nm and 1550.0 nm	✓
Mapping Error	< 2 mm for each actuator	✓
Same optical setup for sphere and asphere test		Only hologram change
Same optical setup in the telescope and lab		✓
Primary focus to beamsplitter distance (MMT physical constraint)	<800 mm	778 mm
Incorporates a phase shifting interferometer		✓
Minimize lens' diameters for cost savings	< 9 inches for doublet	6.5 inches
Minimize beamsplitter diameter		3.5 inches
Coincident pupil plane for both λs		✓
Coincident image plane for both λs		Not achieved
Shimmulator back focal distance equals MMT	9.6 m	Only for infrared 21.8 mm less for visible

Table 1. A comparison between the Shimmulator design requirements and the final design success.

4. Computer Generated Holograms

Early on in the design phase, we realized that computer generated holograms (CGH) would effectively remove the large amounts of spherical aberration caused by the lenses and the secondary mirror. For the aspheric test system, approximately 4000 waves peak-to-valley of spherical aberration at 594 nm were present before the hologram was installed. With the hologram, less than 1/5 of a visible wave of coma remained with no residual spherical aberration. Three holograms were designed for the Shimmulator: one for the adaptive spherical mirror, one for the adaptive aspherical secondary and one for verification purposes. The verification hologram was designed to test the hologram writer's accuracy in the lab before the Shimmulator will be built. All three holograms were designed for simultaneous two wavelength diffraction and manufactured by the Russian Academy of Sciences, Siberian Group.

Another interesting feature designed into the computer generated holograms is multiplexing. Since the system is required to have dual wavelength operation and no element can be changed during testing, the holograms were designed for simultaneous two wavelength diffraction. To accomplish this task, two hologram prescriptions were written over the same central spherical-aberration-removing core and arranged such that each single wavelength hologram pattern alternates with the other pattern. This multiplexing of the two holograms was designed with a constant spacing between the alternating hologram prescriptions. The system imaging requirements demanded a 5.6 arcsecond field referenced back to the sky. Therefore, the hologram spacing for each wavelength was calculated such that the effects of multiplexing would lie outside the 5.6 arcsecond field stop. A 160 μm spacing of the CGH patterns corresponds to a 5.6 arcsecond field at the image plane, therefore, all refracting non-first orders of light will not pass within this physical stop. (wavelength/spacing = 0.589μm/160 μm * diameter_primary / diameter_CGH = 5.6 arcseconds.) Figure 7 illustrates the alternating hologram patterns that incorporate multiplexing by emphasizing the 160 μm spacing between the two holograms in the central core and figure 8 emphasizes the various diffracting order diameters as compared to the physical stop.

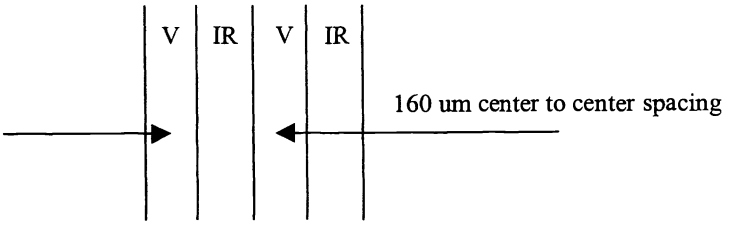

Figure 7. The ability to multiplex two holograms was incorporated by alternating the visible and infrared hologram patterns with a 160 μm spacing between them.

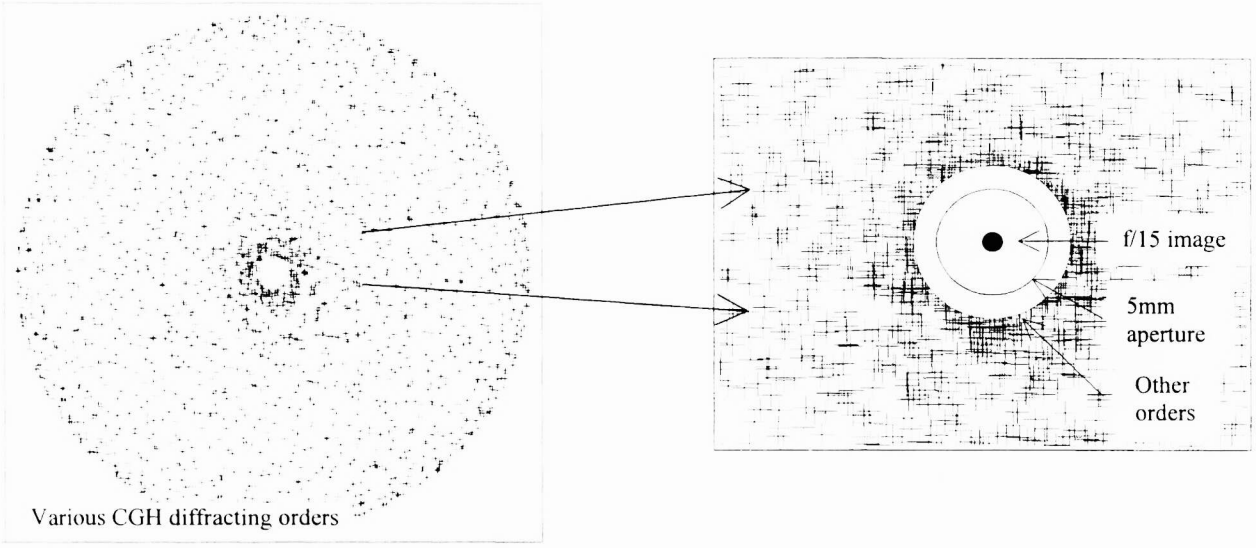

Figure 8. The illustration on the left is a spot diagram of various CGH orders. The enlarged illustration on the right represents the various diameters of the diffracted holographic orders including the 5.6 arcsecond aperture.

The multiplexing of the two holograms presented some difficulties such as crosstalk, a situation that causes stray orders of visible light to refract from the infrared CGH pattern and come to focus within the 5 mm diameter field stop positioned at the MMT f/15 focus. To eliminate this problem, the infrared CGH was left unwritten precisely over this region of overlap over the full inner radius of the main SA correcting section. Figure 9 shows the region where the infrared CGH pattern is left unwritten.

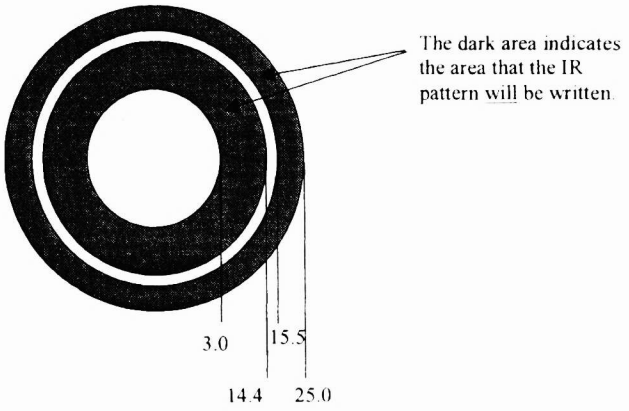

Figure 9. The figure depicts the central spherical aberration hologram for the aspherical test. To avoid the problem of stray visible orders refracting through the infrared pattern, the infrared pattern is not written over the full pupil. The visible pattern is written over the full region from 3.0 mm to 25.0 mm where the infrared pattern is written over two separate regions leaving a void area, precisely vacating the area of crosstalk.

Another advantage employed by the computer generated holograms was the use of alignment patterns. These patterns project a crosshair of diffraction "dots" at precise locations perpendicular to the optical axis to aid in alignment of the most difficult component tolerances. In particular, they will be used for aiding decentration and spacing alignment where the beamsplitter hinders an inside micrometer. Five alignment patterns will be projected by the ring of alternating hologram prescriptions that

surround the central 50 mm spherical aberration corrector. Figure 10 is the fundamental layout of each of the three Shimmulator holograms.

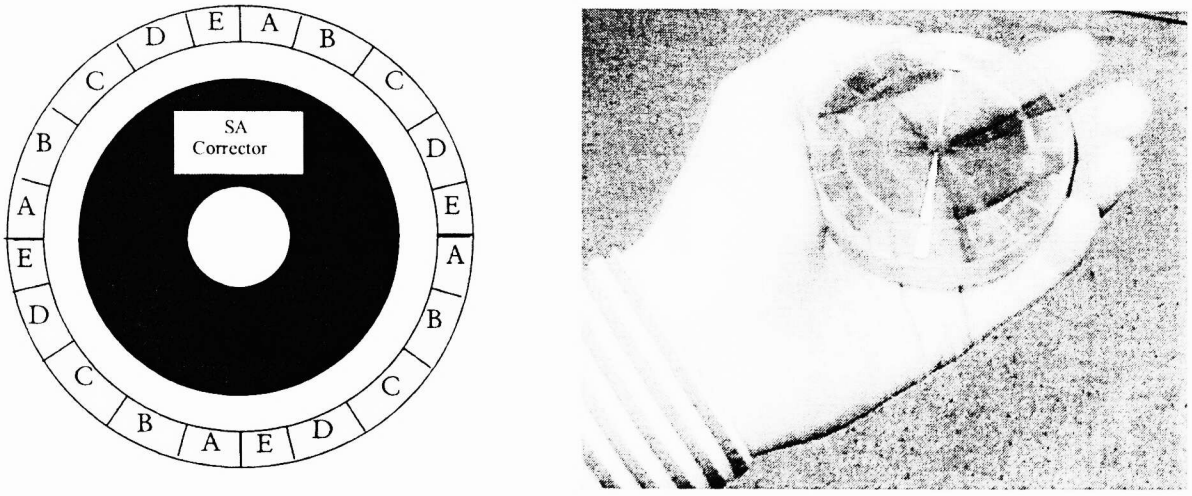

Figure 10. The drawing illustrates the basic hologram layout with the five alignment patterns (named with letters) rotating around the main spherical aberration correcting prescription. Each of the five alignment patterns is written onto the CGH substrate four times with the same pattern alternating a factor of 90 degrees from its "partners". The radial width of the alignment patterns is 6.7 mm and the length of each individual pattern is 8.35 mm with a 1.0 mm spacing between adjacent patterns. On the right is a photo of the actual CGH for the aspheric visible test setup.

Hologram spacing for the aspheric setup is based on the slope of the uncorrected wavefront. Figure 11 is a graph of the sagittal ray fan plots and Figure 12 shows the hologram line spacing vs. pupil radius for the visible hologram prescription. The ray fan plot units are change in slope at the CGH in radians (ray aberration / 15*Diam_cgh) vs. normalized pupil radius.

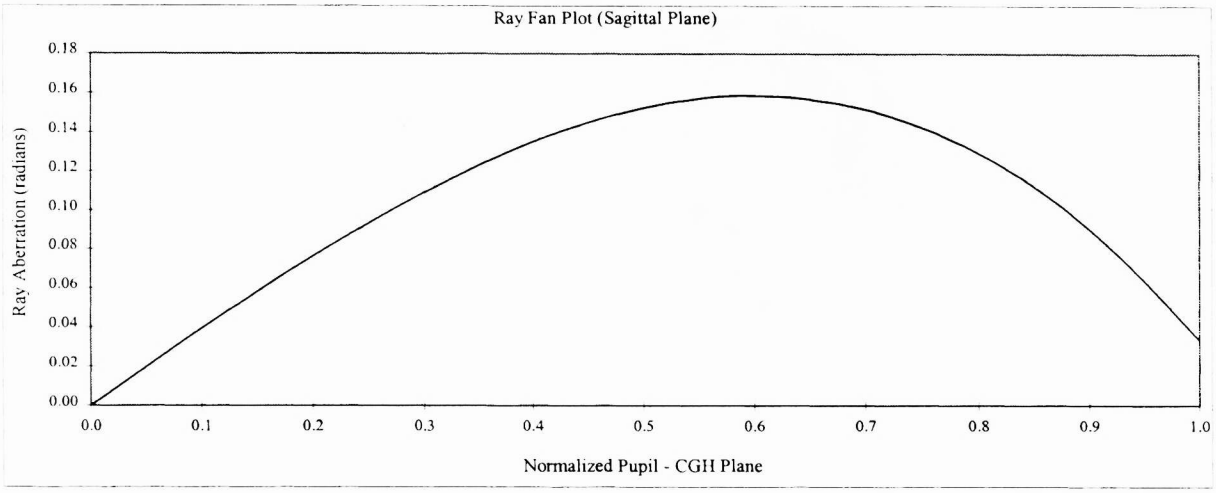

Figure 11. Graphs of the sagittal ray aberration of the non-spherical-aberration-corrected Shimmulator setup for the adaptive secondary asphere with visible illumination.

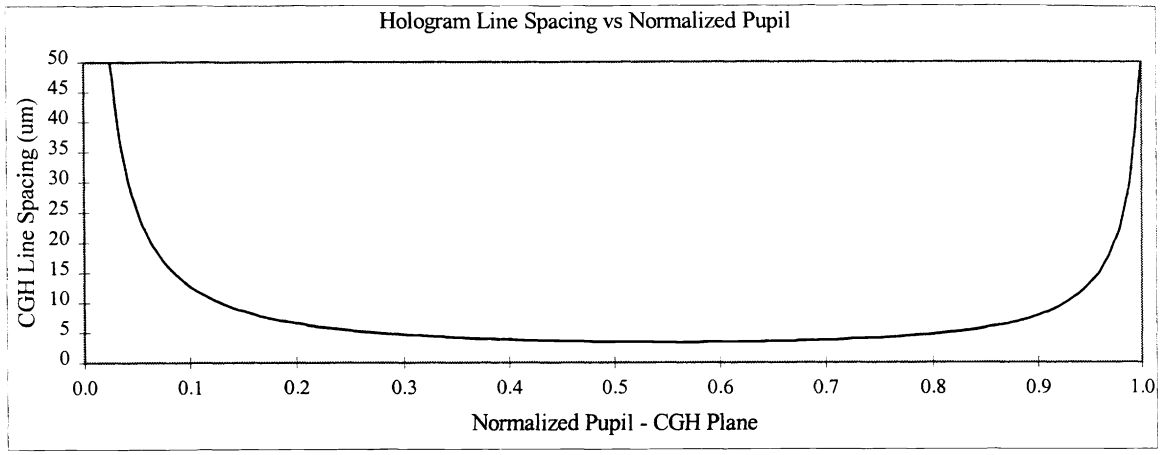

Figure 12. Graph of hologram line spacing needed to correct spherical aberration in the Shimmulator system with visible light for the adaptive secondary asphere.

5. INTERFEROMETER

To test the actuator control system, a phase shifting interferometer has been incorporated into the Shimmulator. The interferometer will be able to measure the adaptive secondary surface shapes as commanded by the software. Since the source for the Shimmulator for both wavelengths will be fiber-fed, the reference path of the interferometer will be coupled to the visible fiber source. The design includes two beamsplitters. The upper beamsplitter reflects the illumination source to the secondary mirror while the lower beamsplitter is positioned 90° to the upper beamsplitter and is used for the interferometer path.

The interferometer is designed for a 594 nm polarized laser source split and coupled to two fibers. One fiber will feed the Shimmulator test system through the upper beamsplitter and represents the interferometer test path. The second phase synced fiber will behave as the reference path and will be interfered with light passing through the upper beamsplitter and reflecting off of the lower beamsplitter for the test path. The interferometer will utilize an electro-opto modulator for phase shifting and a commercial software/hardware package for image acquisition and phase measurement. Figure 13 details the source end of the Shimmulator and its relationship with the interferometer. When the full optical system is installed within the MMT, the doublet, both beamsplitters and the large lenses will rotate in and out of the telescope's main optical axis, for closed-loop testing and sky observing, respectively.

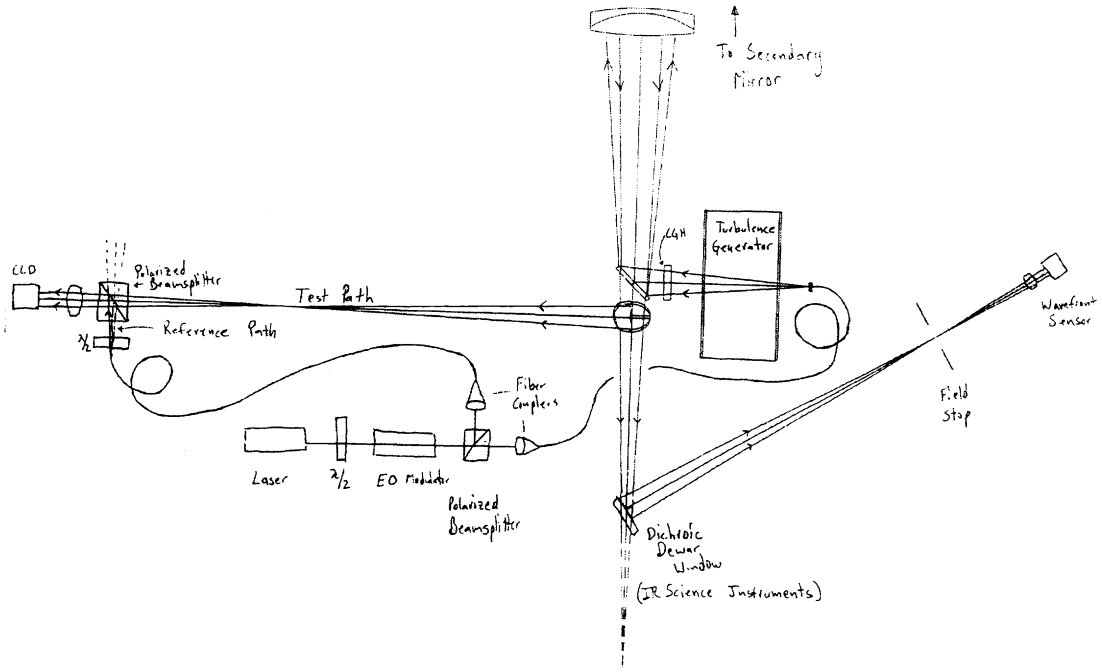

Figure 13. The schematic figure highlights the relationship of the interferometer and the Shimmulator test setup. The interferometer path is rotated 90° to the Shimmulator source path to reduce imparted astigmatism from the two beamsplitters. The laser beam is split into two fibers, one feeds the interferometer path and the other feeds the illumination path.

6. Tolerancing Analysis

Tolerancing analysis has been completed on the nominal design for the aspherical visible system. The analysis revealed some fairly tight tolerances on the doublet including a maximum 0.004 degree wedge for both lenses and a 1 mm tolerance on the spacing for the 8 m path. Furthermore, the tolerancing analysis revealed an expected maximum mapping error of 3.5 mm with an rms wavefront error of 2.2 waves. The total adaptive secondary wavefront compensation is 20 waves, while the mapping error is outside the design specifications of 2 mm.

In order to reduce the expected mapping error without further tightening the manufacturing and alignment tolerances, the doublet axial location was allowed to shift as a compensator for the mapping error. In this manner, the doublet can reduce the mapping error to within the specifications. For this to be accomplished, we are testing the mapping of the Shimmulator by placing physical fiducials onto the secondary mirror. With customized software, we will calculate the optimal doublet position to minimize the mapping error based on the actual manufactured and aligned optical elements.

7. Shimmulator Status

At present, we are in the late stages of manufacturing the custom optical components. The computer generated holograms have been completed and are presently being verified in the lab. The first large lens has already been completed and the second lens is being manufactured at the Steward Observatory Mirror Lab. The doublet is being polished by a local optical fabricator and is near completion. The mapping software for the axial doublet location has not been started.

Three Shimmulator mechanical structures will be constructed, one for testing in the lab, the second for testing in the corner of the telescope chamber and the other for testing within the telescope. The mechanical drawings for both structures are nearing completion and fabrication of the structures will begin soon.

The Shimmulator is expected to begin assembly in the lab starting early January, 1999. The adaptive secondary should be operational and ready for testing in the Shimmulator, May of 1999.

8. ACKNOWLEDGMENTS

Roland Sarlot would like to thank Lucinda Smedley and Patrick McGuire, the reviewers, for their helpful comments and improvements on this paper. In addition, I would like to thank Jim Burge for his continued guidance and teaching.

Work described here has been supported by the Air Force Office of Scientific Research under grant #F49620-96-0366.

9. REFERENCES

1. J. H. Burge, "Applications of computer-generated holograms for interferometric measurement of large aspheric optics" in Optical Fabrication and Testing, Proc. SPIE 2576, 258-269 (1995).
2. V. Cherkashin, et al., "Processing parameter optimization for thermochemical writing of DOEs on chromium films," Proc. SPIE 3010, 168-179 (1997).
3. V.P. Koronkevich, "Laser technologies of diffractive element synthesis for mass-application of optical systems," in Diffractive Optics: Design, Fabrication, and Applications Technical Digest, 1992 (Opt. Soc. Am., Washington, D. C., 1992) 9, pp. 80-81.
4. M. Lloyd-Hart, R. Angel, et al., "Infrared adaptive optics system for the 6.5 m MMT: system status and prototype results", in Proc. SPIE Adaptive Optical Systems Technologies, ed. D. Bonaccini and R.K. Tyson, 3353-32, Kona, Hawaii, March 1998.
5. G. Poleshchuk, "Alignment of diffraction and refraction components in optical systems," Avtometriya, No.6 pp. 27-31 (1985).
6. P. Salinari, and D. G. Sandler, "High-order adaptive secondary mirrors: where are we?", in Proc. SPIE Adaptive Optical System Technologies, ed. D. Bonaccini and R.K. Tyson, 3353-32, Kona, Hawaii, March 1998.

Further author information:
R.J.S. rsarlot@as.arizona.edu, Telephone: 520-626-7252, Facsimile: 520-621-9843
J.H.B. jburge@as.arizona.edu, Telephone: 520-621-8182, Facsimile: 520-621-9843